

UC Davis

UC Davis Previously Published Works

Title

Silicone Oil-Induced Glaucomatous Neurodegeneration in Rhesus Macaques

Permalink

<https://escholarship.org/uc/item/0sn2873t>

Journal

International Journal of Molecular Sciences, 23(24)

ISSN

1661-6596

Authors

Moshiri, Ala

Fang, Fang

Zhuang, Pei

et al.

Publication Date

2022

DOI

10.3390/ijms232415896

Copyright Information



This work is made available under the terms of a Creative Commons Attribution License, available at <https://creativecommons.org/licenses/by/4.0/>

Peer reviewed



Article

Silicone Oil-Induced Glaucomatous Neurodegeneration in Rhesus Macaques

Ala Moshiri ^{1,†}, Fang Fang ^{2,3,†}, Pei Zhuang ^{2,4}, Haoliang Huang ², Xue Feng ², Liang Li ² , Roopa Dalal ² and Yang Hu ^{2,*} 

¹ Department of Ophthalmology & Vision Science, School of Medicine, University of California Davis, Sacramento, CA 95817, USA

² Department of Ophthalmology, Stanford University School of Medicine, Palo Alto, CA 94304, USA

³ Department of Ophthalmology, The Second Xiangya Hospital, Central South University, Changsha 410011, China

⁴ Janssen Research & Development, South San Francisco, CA 94080, USA

* Correspondence: huyang@stanford.edu

† These authors contributed equally to this work.

Abstract: Previously, we developed a simple procedure of intracameral injection of silicone oil (SO) into mouse eyes and established the mouse SOHU (SO-induced ocular hypertension under-detected) glaucoma model with reversible intraocular pressure (IOP) elevation and significant glaucomatous neurodegeneration. Because the anatomy of the non-human primate (NHP) visual system closely resembles that of humans, it is the most likely to predict human responses to diseases and therapies. Here we tried to replicate the mouse SOHU glaucoma model in rhesus macaque monkeys. All six animals that we tested showed significant retinal ganglion cell (RGC) death, optic nerve (ON) degeneration, and visual functional deficits at both 3 and 6 months. In contrast to the mouse SOHU model, however, IOP changed dynamically in these animals, probably due to individual differences in ciliary body tolerance capability. Further optimization of this model is needed to achieve consistent IOP elevation without permanent damage of the ciliary body. The current form of the NHP SOHU model recapitulates the severe degeneration of acute human glaucoma, and is therefore suitable for assessing experimental therapies for neuroprotection and regeneration, and therefore for translating relevant findings into novel and effective treatments for patients with glaucoma and other neurodegenerations.

Keywords: glaucoma; SOHU; neurodegeneration



Citation: Moshiri, A.; Fang, F.; Zhuang, P.; Huang, H.; Feng, X.; Li, L.; Dalal, R.; Hu, Y. Silicone Oil-Induced Glaucomatous Neurodegeneration in Rhesus Macaques. *Int. J. Mol. Sci.* **2022**, *23*, 15896. <https://doi.org/10.3390/ijms232415896>

Academic Editors:

Francine Behar-Cohen and
Dimitra Skondra

Received: 30 October 2022

Accepted: 13 December 2022

Published: 14 December 2022

Publisher's Note: MDPI stays neutral with regard to jurisdictional claims in published maps and institutional affiliations.



Copyright: © 2022 by the authors. Licensee MDPI, Basel, Switzerland. This article is an open access article distributed under the terms and conditions of the Creative Commons Attribution (CC BY) license (<https://creativecommons.org/licenses/by/4.0/>).

1. Introduction

Glaucoma, the most common cause of irreversible blindness, is characterized by progressive peripheral to central loss of retinal ganglion cells (RGCs) and their axons in optic nerve (ON) [1–4]. Although glaucoma can occur at any intraocular pressure (IOP) level [5], elevated IOP is associated with accelerated progression [1–4,6,7]. Lowering IOP is the only available treatment but fails to completely prevent the progression of glaucomatous neurodegeneration [8–11]. Neuroprotectants that promote RGC/ON survival, transplantation of stem cell-derived RGCs to replace lost RGCs, and regeneration therapies to stimulate RGC soma and axon regrowth are promising neural repair strategies to restore vision in glaucoma patients [12,13]. To translate exciting laboratory findings into effective neuroprotective and regenerative treatments, pre-clinical testing in a disease-relevant, translation-enabling animal glaucoma model that closely resembles human patients is critically important.

We recently developed a silicone oil (SO)-induced ocular hypertension under-detected (SOHU) glaucoma mouse model [14–16] based on the well-documented, SO-induced human secondary glaucoma that occurs as a complication of vitreoretinal surgery [17,18].

By blocking aqueous flow to the anterior chamber with a single intracameral injection of SO that induces pupillary block, this SO injection causes accumulation of aqueous and significant IOP elevation in the posterior chamber, and subsequent progressive RGC and ON degeneration. Importantly, the ocular hypertension of the SOHU model can be reversed quickly and definitively by easily removing SO from the anterior chamber [14–16]. However, there is a recognized gap in the translation of successful neuroprotective and regenerative therapies identified in rodent models of glaucoma to treatment for glaucoma patients. Rodents have known limitations that may impede translation of potential therapeutics: differences in immune system responses, ON head (ONH) architecture, and brain structures and circuitry may contribute to differences in pathogenesis between rodents and primates and, therefore, to critically different responses to therapeutics. Despite the many benefits of the mouse SOHU model, a higher experimental animal species is needed for pre-clinical translation research.

The anatomy of the non-human primate (NHP) visual system closely resembles that of humans and includes a similar distribution of rods and cones, a specialized macula and fovea and lamina cribrosa not present in rodent, comparable contrast sensitivity and visual acuity, and almost identical retinocortical architecture [19,20]. An NHP glaucoma model is the most likely to predict human responses to ocular hypertension and therapies, and the rhesus macaque monkey has been used successfully in experimental glaucoma research [21,22]. Since SO-induced pupillary block causes secondary glaucoma in both human patients and mice, we reasoned that the same procedure may be adapted to different animal species with minimal confounding factors. Here we report the development of a novel NHP glaucoma model in rhesus macaque monkeys, in which intracameral SO injection causes severe RGC and ON degeneration and visual function deficits. We expect this model to be useful for studying primate RGC pathophysiology, assessing experimental neuroprotective and regenerative therapies, and therefore for translating relevant findings into novel and effective treatments for patients with glaucoma and other neurodegenerations.

2. Results

2.1. Intracameral Injection of SO in Rhesus Macaque Monkey Causes RNFL Thinning and Decreases PhNR

We injected roughly 100 μ L SO into the anterior chamber of the right eyes of 6 macaque monkeys (Table 1), filling 80% SO of the anterior chamber with complete covering of the pupil (Figure 1A). Retinal morphology and function were assayed before SO injection and at different time points after. These assays included fundus imaging, spectral-domain optical coherence tomography (SD-OCT), and electroretinography (ERG) (Figure 1B). Thinning of the retina nerve fiber layer (RNFL) measured by OCT is used clinically as a biomarker for RGC/ON degeneration [23–25]. We measured the RNFL thickness of the animals and detected significant thinning of RNFL in the SOHU eyes at 6-month post injection (6 mpi) but not at 3 mpi (Figure 2A,B), indicating inner retina neurodegeneration. We also examined the visual function of these macaques. The photopic negative response (PhNR) of the photopic full-field ERG is a negative-going wave that occurs after the b-wave in response to a brief flash and reflects the function of RGCs and their axons in general. Its amplitude is reduced early in human glaucoma [26], which also correlates well with structural loss in NHP glaucoma [27]. Both b-wave and PhNR's amplitudes decreased in the SOHU eyes at all time points after SO injection, but only reached statistical significance at 1 mpi (Figure 2C), suggesting functional deficits of the inner retina.

Table 1. Animal Information.

| ID | Sex | Date of Birth | Weight (Kg) |
|-------|-----|-------------------------|-------------|
| 38361 | F | 10 May 2007 (13 years) | 9.68 |
| 42946 | F | 31 May 2012 (8 years) | 9.91 |
| 44193 | M | 06 April 2014 (7 years) | 9.16 |
| 44639 | M | 28 May 2014 (7 years) | 12.95 |
| 44876 | F | 11 May 2015 (6 years) | 10.38 |
| 45513 | M | 22 June 2015 (6 years) | 8.43 |

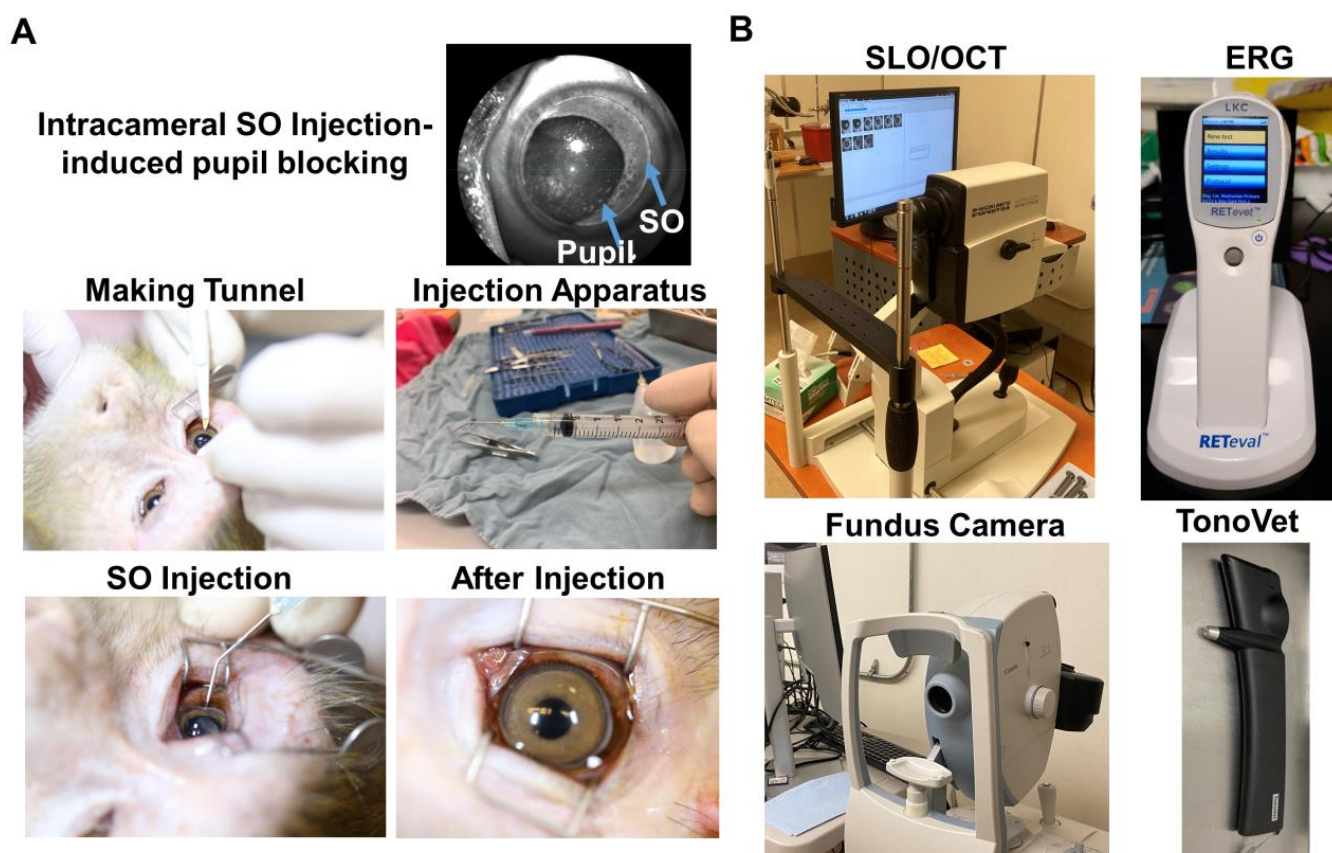


Figure 1. Intracameral SO injection and in vivo assays of rhesus macaque monkey eyes. (A) The procedures of SO intracameral injection in monkey eye; (B) The equipment used for in vivo assays, including SLO/OCT, ERG, fundus imaging, and TonoVet for IOP measurement.

2.2. Significant RGC and ON Degeneration of the SOHU Eyes at 3 mpi and 6 mpi in All Tested Animals

To confirm the glaucomatous neurodegeneration, we euthanized two animals at 3 mpi and four animals at 6 mpi for histological analysis of post-mortem retina and ON. Consistent with the in vivo structural and functional deficits detected in the living animal, retinal wholemounts revealed significant RGC somata loss in the SOHU eye throughout the peripheral to the central retinas at both 3 mpi and 6 mpi (Figure 3A,B); and semithin cross-sections showed significant RGC axon degeneration in ON at both 3 mpi and 6 mpi (Figure 3C,D), indicating significant glaucomatous neurodegeneration of the SOHU eyes.

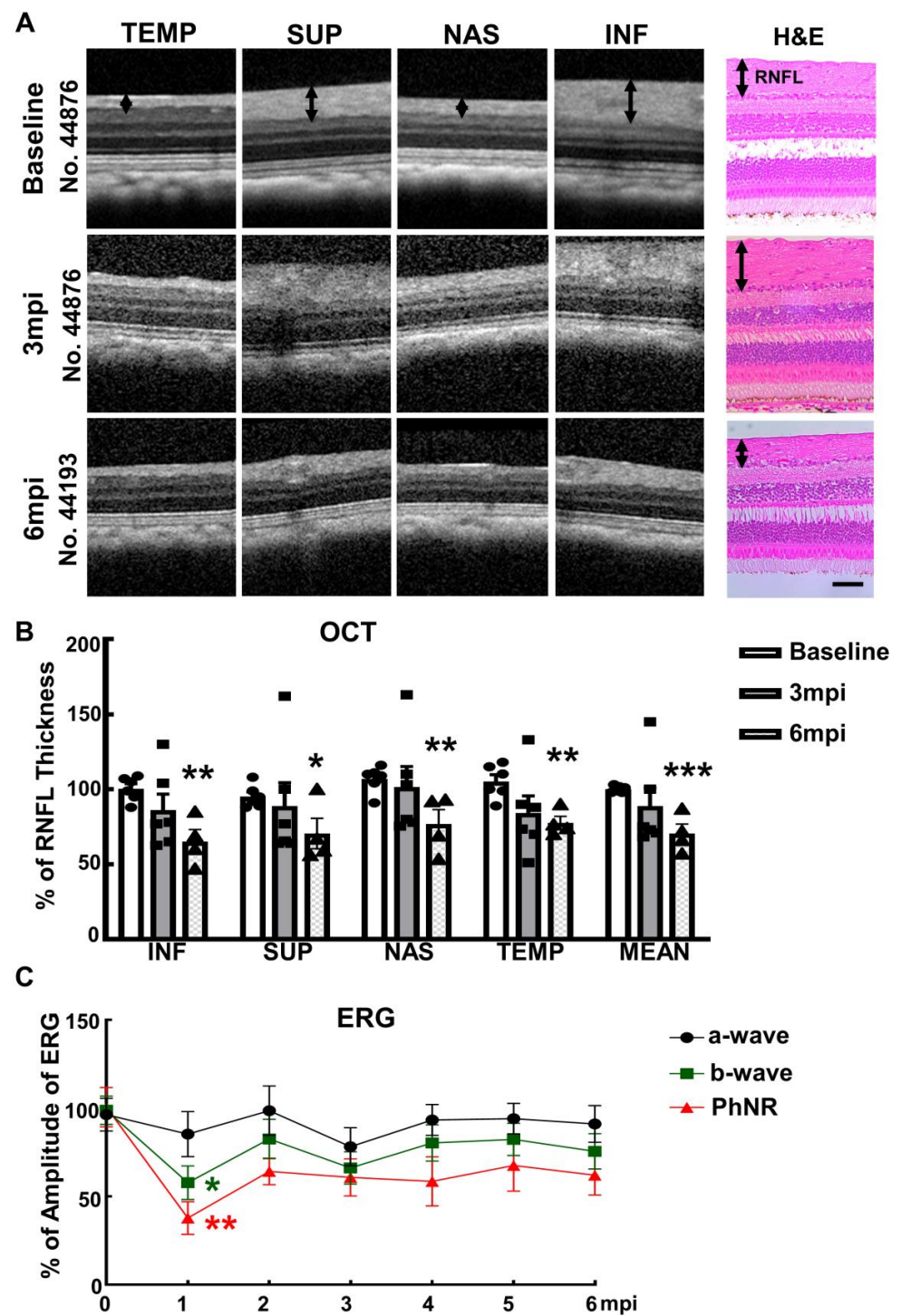


Figure 2. Visual function and morphological deficits of SOHU monkey eyes. (A) Longitudinal SD-OCT imaging of SOHU retinas at inferior (INF), superior (SUP), nasal (NAS), and temple (TEMP) quadrants; and the H & E staining of retina sections; (B) Measurements of RNFL thickness at different time points, represented as percentage of SOHU eyes compared to CL eyes. Data are presented as means \pm s.e.m, $n = 6$ for 3 mpi and $n = 4$ for 6 mpi, *: $p < 0.05$, **: $p < 0.01$, ***: $p < 0.001$, Student's t test; (C) Longitudinal ERG recording of macaque eyes at different time points after SO injection and the measurements of the amplitudes of a wave, b wave and PhNR, represented as percentage of the amplitudes in the SOHU eyes, compared to the CL eyes. Data are presented as means \pm s.e.m, $n = 6$ for 1–3 mpi and $n = 4$ for 4–6 mpi, *: $p < 0.05$, **: $p < 0.01$, One-way ANOVA with Tukey's multiple comparison test.

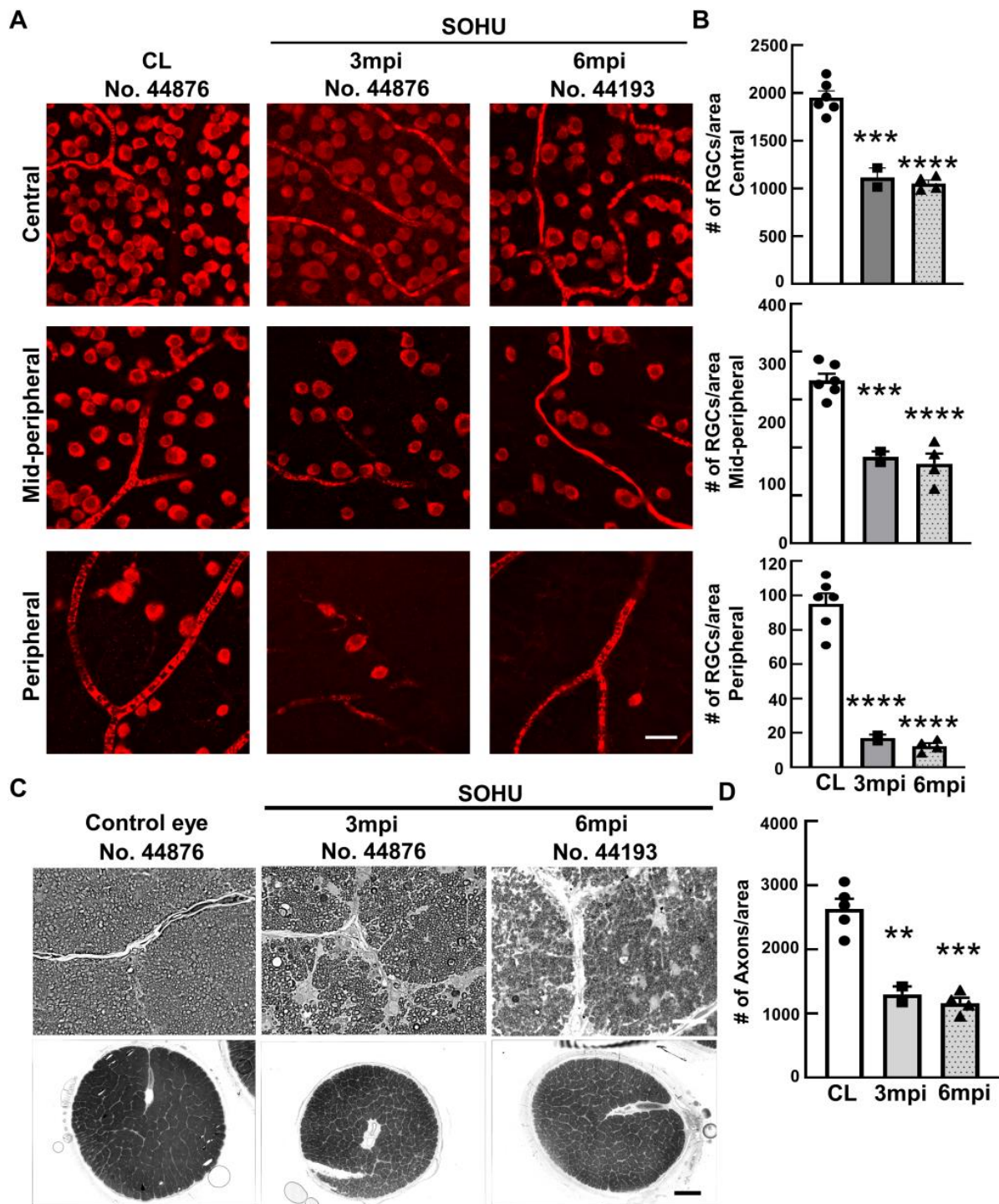


Figure 3. Severe RGC and ON degeneration in SOHU eyes at 3 mpi and 6 mpi. (A) Confocal images of wholemount retinas showing surviving RBPMS-positive (red) RGCs in the peripheral, mid-peripheral, and central retina at 3 and 6 mpi. Scale bar, 20 μ m; (B) Quantification of surviving RGCs in the peripheral, mid-peripheral, and central retina. CL: contralateral control eyes. Data are presented as means \pm s.e.m, $n = 2$ (No. 44876 and No. 45513) for 3 mpi and $n = 4$ for 6 mpi, ***: $p < 0.001$, ****: $p < 0.0001$, one-way ANOVA with Tukey’s multiple comparison test; (C) Light microscope images of semi-thin transverse sections of ON stained with PPD in the corresponding groups. Upper panel: 100 \times , Scale bar, 20 μ m; lower panel: 60 \times , Scale bar, 500 μ m; (D) Quantification of surviving RGC axons in ON. Data are presented as means \pm s.e.m, $n = 2$ for 3 mpi and $n = 4$ for 6 mpi, **: $p < 0.01$, ***: $p < 0.001$, One-way ANOVA with Tukey’s multiple comparison test.

2.3. Dynamic IOP Changes in the SOHU Macaque Eyes Associated with Ciliary Body Atrophy

Surprisingly, these macaques showed different IOP dynamics after SO injection. In two animals (#44876 and #45513), IOP was elevated immediately after SO injection (15 to 19 mmHg and 13 to 22 mmHg, Figure 4A). Because restrictions of the Primate Center then precluded measuring the IOPs before 1 mpi or more frequently than once a month thereafter, we could not measure the IOP earlier or more often. Therefore, we do not know for the duration of the transient IOP elevation after SO injection. However, all six animals showed substantial ocular hypotension at 1 mpi and 2 mpi: IOPs of the SOHU eyes were much lower than their baselines or their contralateral control eyes (Figure 4A,B). The ocular hypotension lasted from 1 mpi to 3 mpi in two animals (#44876 and #45513) and from 1 mpi to 5 mpi in one animal (#44639); IOP returned progressively to normal between 2–6 mpi in three animals (#42946, #44639, and #44193) that we maintained for 6 months. In one animal (#38361) IOP was much higher than normal from 3–5 mpi, at first fell significantly when SO was removed from the eye at 5 mpi, then returned to normal one month later. The sequence of changes in this animal indicated that the SO-induced pupillary blocking was the cause of IOP elevation, and that simply removing the SO reversed the pupillary blocking and ocular hypertension. Because we missed the measurement at the 2 mpi time point for this animal (#38361), we assume that the IOP of the SOHU eye recovered from ocular hypotension and became elevated between 1 mpi and 3 mpi.

We suspect that the pupillary blockade caused a substantial elevation of the IOP acutely, which led to ciliary body “shutdown”, as in some human patients [28]. The subsequent lasting ocular hypotony then happened due to ceased aqueous production from ciliary body. Indeed, the ciliary body was severely atrophied in the SOHU eyes of all animals, revealed by H & E staining of the anterior segments of the eyes (Figures 5 and S1A). Interestingly, the ciliary body atrophy of animal 38361 was much milder than that of the other animals (Figure 5B), consistent with ciliary body recovery and IOP elevation at 3–5 mpi after initial hypotension at 1 mpi (Figure 4A). There was no inflammation or obvious deformation of cornea, sclera, iris, or lens, although the pupils of the SOHU eyes were fixed in the mid-dilated state (Figure S1B), suggesting a transient high IOP elevation, which may result in ischemic iris sphincter muscle and consequently limitation in constriction, as in patients with acute angle closure glaucoma [29].

2.4. ON Head “Cupping” Is Present in the SOHU Eye with Persistent IOP Elevation

A characteristic morphological feature of human glaucoma is enlargement of the depression in the center of the ONH, called glaucomatous “cupping” [30,31]. Strikingly, live fundus imaging with confocal scanning laser ophthalmoscopy (cSLO) readily detected this signature morphological change of glaucoma in the SOHU macaque eye (#38361) by at 3 and 5 mpi (Figure 6A), corresponding to IOP elevation (Figure 4). That ONH cupping is absent in the mouse SOHU model further confirms the similarity between macaque and human eyes. This characteristic glaucomatous optic cup enlargement was even more obvious in OCT live imaging by radial B-scan centered through the ONH (Figure 6B). Based on previously developed measurement of the anatomic features of the macaque ONH [31,32], we applied the Visualization Toolkit (VTK) to reconstruct and delineate the OCT imaging data (Figure S2A). We used inner limiting membrane (ILM), Bruch’s membrane opening (BMO), the two discrete points at either side of the neural canal, and the BMO reference plane as references to acquire minimum rim width (MRW), rim volume (RimV), and cup volume (CupV). Obvious shortening of MRW, shrinking of RimV, and enlarging of CupV were detected in the SOHU eye compared to contralateral control eye (Figure S2B). The H & E staining of the ONH confirmed the “cupping” phenotype and significant thinning of RNFL (Figure S2C–E). The lamina cribrosa is a trabecular connective tissue to support RGC axons at the ONH [33]. Its deformation, such as increased curve and depth, may correlate with RNFL thinning in glaucoma patients [34,35]. Interestingly, collagen staining of the ONH of the SOHU eye also showed lamina cribrosa bowing (Figure S2D). ONH “cupping” cannot be found by fundus SLO images or OCT images in

the eyes of the other macaques without persistent IOP elevation (Figure S3), indicating the correlation of prolonged ocular hypertension and ONH “cupping”.

A
IOP measurement (mmHg)

| SOHU | 44876 | | 45513 | | 42946 | | 44639 | | 44193 | | 38361 | |
|----------------------------|-------|----|-----------------|----|-------|----|-------|----|-------|----|-------|----|
| | SOHU | CL | SOHU | CL | SOHU | CL | SOHU | CL | SOHU | CL | SOHU | CL |
| Pre-Injection | 15 | 18 | 13 | 12 | 9 | 9 | 13 | 12 | 11 | 14 | 17 | 16 |
| Post-injection immediately | 19 | 18 | 22 | 11 | 11 | 9 | 11 | 12 | 9 | 14 | | |
| 1mpi | 4 | 16 | Too low to read | 14 | 6 | 11 | 8 | 17 | 5 | 11 | 11 | 19 |
| 2mpi | 3 | 16 | 3 | 12 | 9 | 9 | 8 | 12 | 10 | 14 | | |
| 3mpi | 2 | 11 | 3 | 11 | 8 | 9 | 8 | 16 | 12 | 14 | 49 | 18 |
| 4mpi | | | | | 12 | 10 | 9 | 13 | 13 | 15 | | |
| 5mpi | | | | | 9 | 6 | 8 | 12 | 12 | 11 | 36 | 18 |
| SO removal | | | | | | | | | | | 9 | 19 |
| 6mpi | | | | | 12 | 14 | 10 | 12 | 13 | 14 | 15 | 17 |

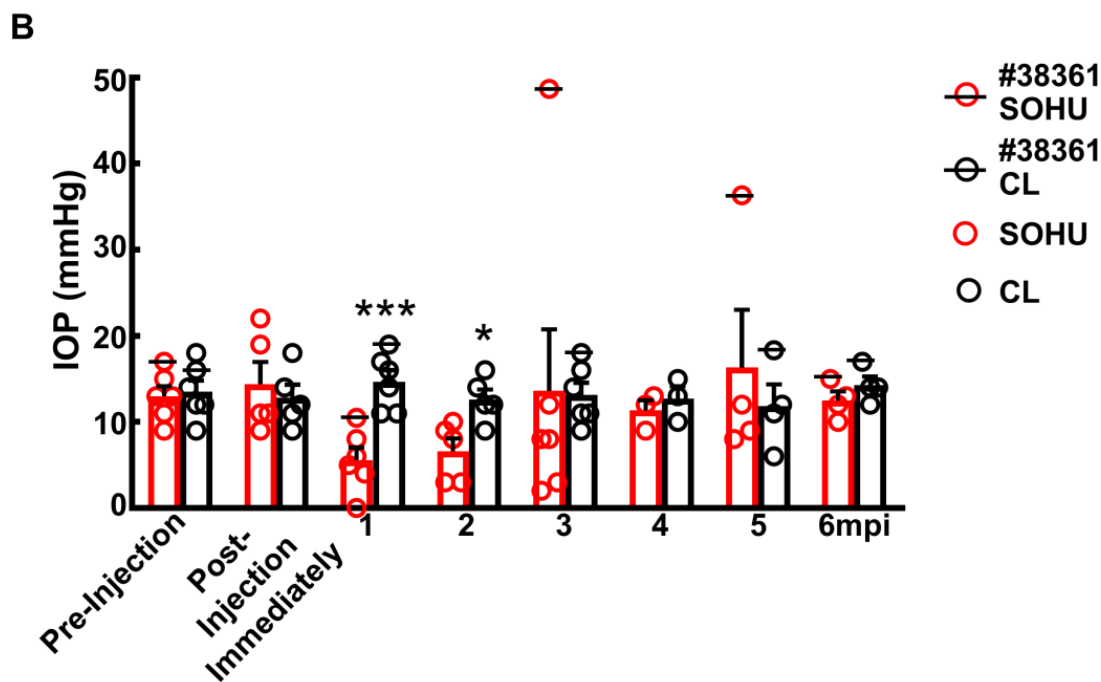


Figure 4. Dynamic IOP changes of SOHU eyes. Table (A) and Bar graph (B) presentation of longitudinal IOP measurements of experimental (SOHU) eyes and contralateral control (CL) eyes at different time points after SO injection. mpi: month post injection. Data are presented as means \pm s.e.m, $n = 6$ (1–3 mpi) and $n = 4$ (4–6 mpi) of each group; *: $p < 0.05$, ***: $p < 0.001$, Student’s t test. Red-coded numbers are lower than normal and green-coded numbers are higher than normal IOP.

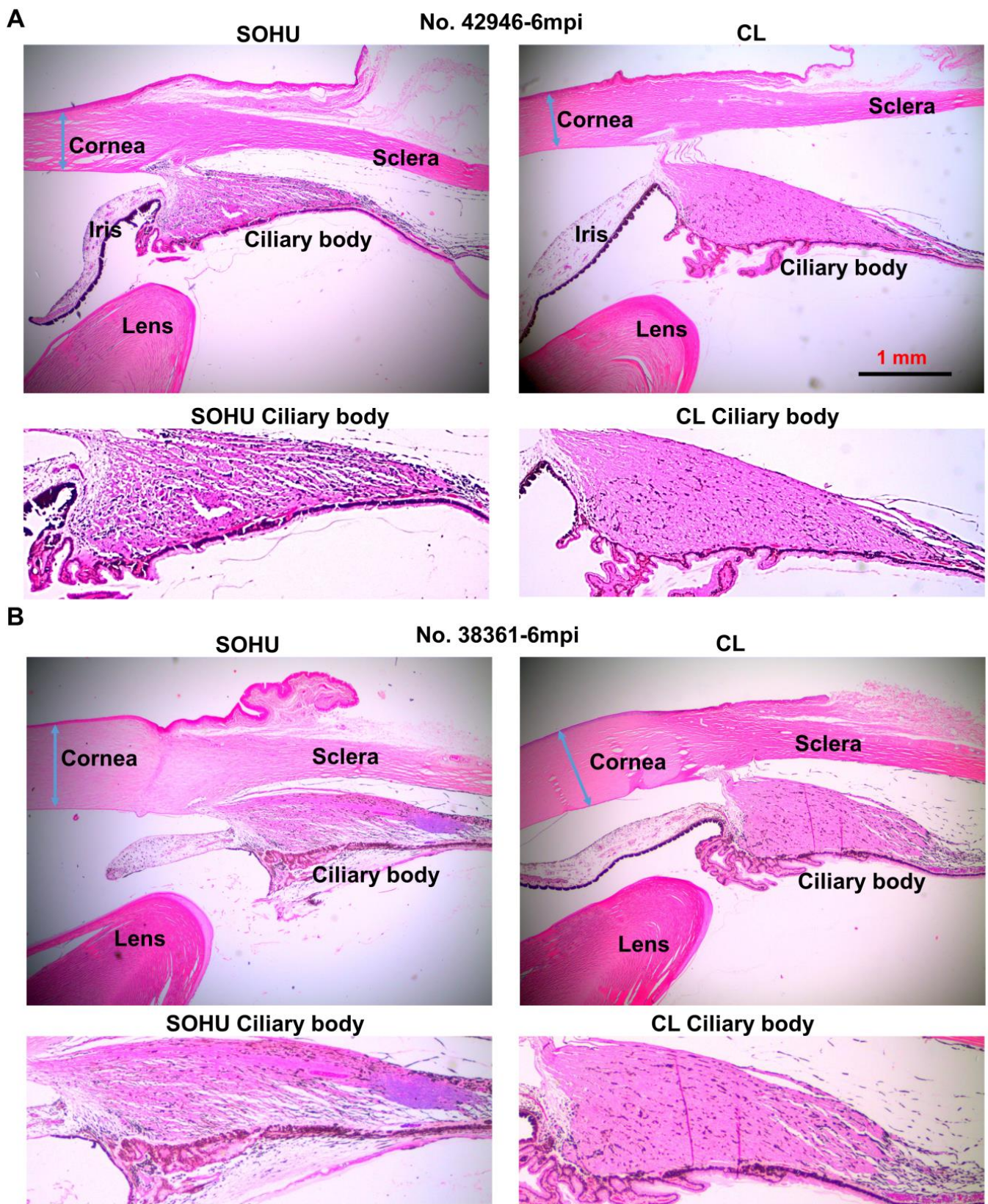


Figure 5. Ciliary body atrophy in SOHU eyes at 6 mpi. (A) Animal No. 42946; (B) Animal No. 38361. Anterior chamber sections stained with H & E and imaged with 2× lens; and enlarged images of ciliary body, showing loose arrangement, larger interfibrous areas, and increased cellular invasion in muscle fibers.

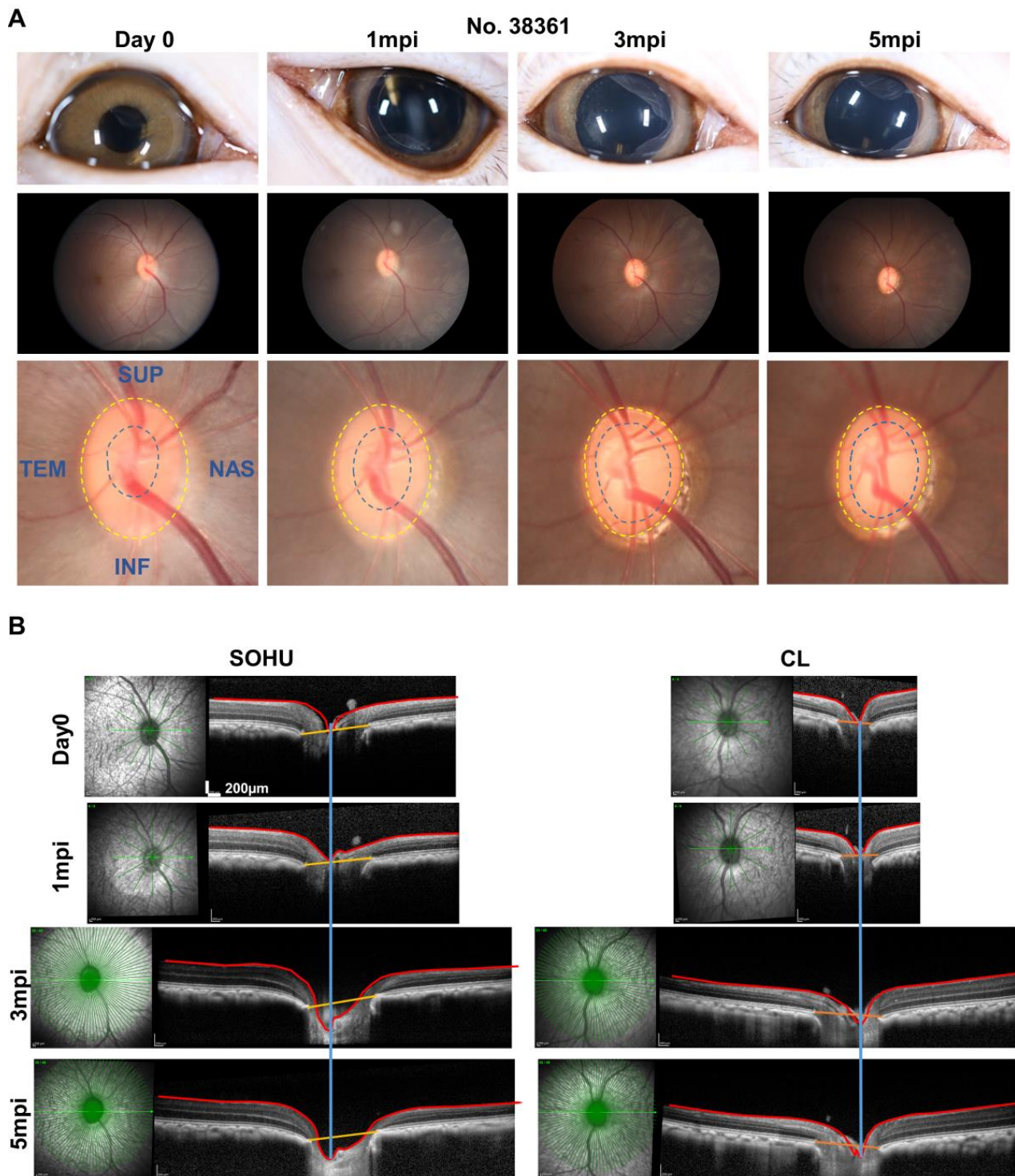


Figure 6. ONH “cupping” in animal #38361 associated with IOP elevation. (A) The retinal fundus images of the SOHU eye before and after SO injection. Yellow dotted line outlines the optic disc; blue dotted line outlines optic cup; (B) Longitudinal SD-OCT imaging of macaque ON head with 48 radial B-scans acquired over a 30° area at 768 A-scans per B-scan, ART = 16 repetitions.

3. Discussion

The present report establishes a straightforward and minimally invasive procedure, a single intracameral injection of SO, to induce reproducible glaucomatous RGC and ON degeneration within 3–6 months in rhesus macaque monkeys. The model mimics

acute secondary glaucoma caused by pupillary blocking and can be used to study the pathogenesis of neurodegeneration and to select urgently needed neuroprotectants and regeneration therapies that are unrelated to IOP management. Within 3–6 months of a simple SO intracameral injection, the SOHU eyes of all monkeys studied showed a highly consistent array of findings: significant thinning of RNFL, decreased visual function (PhNR), and loss of RGC somata and axons. The reversible intracameral SO injection does not cause overt anterior ocular structural damage other than the ciliary body while simulating acute glaucomatous RGC and ON changes. Therefore, this inducible, reproducible, and clinically relevant NHP neurodegeneration model can be used to decipher the molecular mechanisms of transient ocular hypertension-induced glaucomatous degeneration in primate, and to preclinically assess the efficacy and safety of experimental strategies for neuroprotection and regeneration.

A unique feature of this NHP model is the transient IOP elevation-induced ciliary body “shock”. Unlike mouse, but as can happen in humans [28], the NHP ciliary body seems very vulnerable to acutely elevated IOP, which first caused it to stop generating aqueous humor and ocular hypotension, and ultimately leads to atrophy. All six monkeys that we tested consistently developed persistent intraocular hypotension at 1 mpi, and histological evidence of ciliary body atrophy, although we captured the initial transient IOP elevation before ocular hypotension in only two animals. One animal (No. 38361) recovered normal ciliary body function between 1–3 mpi and, therefore, generated and maintained an elevated IOP at 3–5 mpi, until we removed SO. Removal allowed IOP to return to normal. Damage of this animal’s ciliary body consistently seemed much milder than in other animals. Unfortunately, most animals (five out of six monkeys) studied did not fully recover normal ciliary body function. Ciliary body function appeared to recover in part in some of the animals, however, since they became able to maintain low or normal IOP in the presence of SO-induced pupillary blocking within the time period of the experiment (3–6 months). Despite the absence of long-lasting chronic ocular hypertension, all five animals showed similar RGC and ON degeneration as the one animal with persistent ocular hypertension. This suggests that transient acute IOP elevation causes the neurodegeneration. From our mouse study [16], we learned that although SO removal allows IOP to return quickly to normal, it does not stop the progression of glaucomatous neurodegeneration in the SOHU model. This result is also consistent with the clinical observation that visual field loss can progress aggressively in some glaucoma patients whose IOP is maintained at a relatively low level. Thus, this NHP SOHU model can be used to determine the efficacy of experimental neuroprotection treatment when IOP is low after an initial period of pathogenic ocular hypertension, simulating clinical IOP treatment. Advanced retinal imaging and visual function assays that are available for humans can be applied to this primate glaucoma model. These assays will identify morphological and functional changes in RGCs and ON that can serve as potential biomarkers in glaucoma and other optic neuropathies. Since optic neuropathy can also be associated with other central nervous system (CNS) neurodegenerative diseases [36], including multiple sclerosis [23,37,38], Alzheimer’s disease [39,40], and amyotrophic lateral sclerosis [41,42], this model may be broadly applicable to diverse CNS degenerative diseases.

One animal (#38361) was able to recover rather quickly from ciliary body shock and resume adequate aqueous humor production, which increased IOP due to pupillary blocking. It is notable that the characteristic glaucomatous ONH “cupping” was associated with persistent ocular hypertension in this animal but absent from the other animals without persistent IOP elevation. We do not know what causes the variable ciliary body responses of different animals. Age may play a role since #38361 was much older (13 years) than the other five animals (6–8 years); the middle-aged ciliary body in this animal may be more resilient than younger ciliary bodies. Further systematic studies with additional senior, middle-aged, and young NHP animals are needed to clarify the reasons and to further optimize this model. For example, a modified SOHU model like the one that we developed in mouse that induces and maintains a moderate elevation of IOP through

frequent pupil dilation [16] may prevent the acute severe IOP elevation causing ciliary body shock. The initial IOP elevation after SO injection may be directly related to ciliary body damage. Future studies using different amounts of SO to produce various degrees of partial pupil blocking may allow us to optimize this model to generate milder IOP elevation without ciliary body damage, which will produce an even more advantageous ocular hypertension glaucoma model.

4. Materials and Methods

Animal. The animals in this study were rhesus macaques (*Macaca mulatta*) born and maintained at the California National Primate Research Center (CNPRC). The CNPRC is accredited by the Association for Assessment and Accreditation of Laboratory Animal Care (AAALAC) International. Guidelines of the Association for Research in Vision and Ophthalmology Statement for the Use of Animals in Ophthalmic and Vision Research were followed. All aspects of this study were in accordance with the National Institutes of Health (NIH) Guide for the Care and Use of Laboratory Animals and all methods are reported in accordance with ARRIVE guidelines. Phenotyping and ophthalmic examinations were performed according to an animal protocol approved by the University of California Davis Institutional Animal Care and Use Committee and Stanford University School of Medicine.

Intracameral injection of SO. The procedure is similar to the published protocol [14,15] but with modification for monkey eyes. Sedation was achieved by intramuscular injection of ketamine hydrochloride (5–30 mg/kg IM) and dexmedetomidine (0.05–0.075 mg/kg IM). The eyes were prepped in a usual sterile fashion for ophthalmic surgery including topical anesthetic 0.5% proparacaine hydrochloride (Akorn, Somerset, NJ, USA) followed by 5% betadine to the ocular surface and adnexa. A disposable 15-degree blade was used to make a side-port incision at the corneal limbus to enter the anterior chamber inferiorly near the 6 o'clock position in order to minimize the likelihood of oil leaking out of the eye. Silicone oil (SO, 1000 mPa.s, Silikon, Alcon Laboratories, Fort Worth, TX, USA) in a 3 cc syringe on a bent 25 gauge cannula was introduced into the anterior chamber. SO was injected little by little, stopping intermittently with gentle pressure applied to the posterior aspect of the limbal incision to allow for aqueous humor to exit the eye. Oil was injected to fill the anterior chamber to a physiologic depth with roughly ~70–80% silicone oil and to cover the entire pupil with ~100 µL volume. After the injection, the wound was tested to insure it was self-sealing and veterinary antibiotic ointment (BNP Ophthalmic Ointment, Vetropolycin, Dechra, Overland Park, KS, USA) was applied to the surface of the injected eye. The contralateral control eyes received a mock injection with no penetration of the eye. Animals were monitored by a trained technician and a veterinarian at all times.

Removing SO from the anterior chamber. The procedure is similar to the published protocol [14,15] with modification for monkey eyes. Briefly, after the animal was anesthetized the eye was prepped in a sterile fashion as above. A superior (12 o'clock) corneal side-port incision was made using a 15-degree blade at the corneal limbus. A 3 cc syringe filled with sterile balanced salt solution (BSS Plus, Alcon Laboratories, Ft. Worth, TX, USA) with a 25 gauge bent cannula was introduced into the anterior chamber and saline was gently injected little by little while periodically allowing oil to egress from the same incision by gently applying pressure to the posterior aspect of the wound. After removing all of the oil and replacing it incrementally with BSS to a physiologic depth, the cannula was removed and the wound was checked to be self-sealing, after which antibiotic ointment was applied.

Eye examinations and retinal fundus imaging. Sedated ophthalmic examination included measurement of intraocular pressure (IOP) using rebound tonometry (Icare TA01i, Finland) while the animal was held upright and with careful attention not to apply any pressure to the globe. Three IOP measurements were taken and averaged at each exam date. Examination also included pupillary light reflex testing, external and portable slit lamp examination, as well as dilated (Tropicamide 1%, Phenylephrine 2.5%, Cyclopentolate 1%) indirect ophthalmoscopy. Sedation was achieved by intramuscular injection of ketamine

hydrochloride (5–30 mg/kg IM) and dexmedetomidine (0.05–0.075 mg/kg IM). Animals were monitored by a trained technician and a veterinarian at all times. Color and red-free fundus photographs were obtained with the CF-1 Retinal Camera with a 50° wide angle lens (Canon, Tokyo, Japan).

Spectral-domain optical coherence tomography (SD-OCT) imaging. SD-OCT with confocal scanning laser ophthalmoscopy (cSLO) was also performed (Spectralis® HRA+OCT, Heidelberg, Germany). High-resolution radial and circumferential scans centered on the optic nerve were obtained using a corneal curvature (K) value of 6.5 mm radius. For the high-resolution radial scans of the optic nerve head (ONH), 48 radial B-scans were acquired by 870 nm SD-OCT (Spectralis; Heidelberg Engineering, GmbH), over a 30° area, and 768 A-scans per B-scan at ART = 16 repetitions. All repetitive scans were acquired using eye-tracking and averaged to reduce speckle noise. We read in all the images and measured MRW, RimV, and CupV using R program. The codes that we used to calculate MRW, RimV and CupV are at Github (Available online: <https://github.com/HuLab-Code/ONHV> (accessed on 21 May 2022)). For each monkey eye, the center of the ONH was estimated and registered during the first imaging session and used to align all follow-up images. All imaging was done by the same ophthalmic imaging team. All OCT images were taken through the center of the pupil. Speculums were used and corneal hydration was maintained through application of topical lubrication (Gentel artificial tears) approximately every 1–2 min during imaging sessions. The en-face retinal images were captured with the Heidelberg Spectralis SLO/OCT system equipped with an 870 nm infrared wavelength light source and a 30° lens (Heidelberg Engineering). The average thickness of retinal nerve fiber layer (RNFL) around the optic nerve head was measured manually with the aid of Heidelberg software. The investigators who measured the thickness of RNFL were masked to the treatment of the samples.

Electroretinography (ERG) recording. After dilation, a full-field ERG (ffERG) containing six different tests was performed on each eye following a 30-min dark adaptation period. ERG-Jet electrodes (item #95-011) were coupled with the RETeval instrument (LKC Technologies, Gaithersburg, MD, United States), as previously described [43]. A standard flash electroretinogram was performed according to the approved protocol of the International Society for Clinical Electrophysiology of Vision (ISCEV). There were four dark adapted tests (0.01 cd × s/m², 3.0 cd × s/m², 10.0 cd × s/m², and oscillatory potentials 3.0 cd × s/m²). After 10 min of light adaptation, two additional tests were performed (3.0 cd × s/m² single flash with measurement of the photopic negative response and photopic flicker 3.0 cd × s/m²). Both time (ms) and amplitude (μV) were obtained for each test on each eye. Single flash tests measured an a-wave and b-wave. Oscillatory potentials measured five wave points and a sum. In the photopic flicker test, the first wave point is reported. Measurements were recorded and displayed using the manufacturer's software.

Immunohistochemistry of whole-mount retina and RGC counting. The detailed procedure has been published before [14,15,44] with modification to accommodate large monkey eyes. Briefly, after intravitreal injection with 10% formalin in PBS, the eyes and optic nerves were dissected out, post-fixed with 10% formalin for 24 h at room temperature. Retinas were dissected out and washed extensively in PBS before blocking in staining buffer (10% normal goat serum, Sigma-Aldrich, and 2% Triton X-100 in PBS) for half an hour. RBPMS guinea pig antibody made at ProSci Inc (Poway, California) according to publications [45,46] was diluted (1:4000) in the same staining buffer. Floating retinas were incubated with primary antibodies overnight at 4 °C and washed 3 times for 30 min each with PBS. Secondary antibodies (Cy3) were then applied (1:200; Jackson ImmunoResearch, West Grove, Pennsylvania) and incubated for 1 h at room temperature. Retinas were again washed 3 times for 30 min each with PBS before a cover slip was attached with Fluoromount-G (SouthernBiotech, Birmingham, Alabama). For RGC counting, whole-mount retinas were immunostained with the RBPMS antibody, 6 fields sampled from each region (periphery, mid-periphery, and center retinas) using a 20× lens with Keyence epifluorescence microscope, and RBPMS⁺ RGCs of each image (540 μm × 720 μm) were

counted manually with Fiji/ImageJ. The investigators who counted the cells were masked to the treatment of the samples.

ON semi-thin sections and quantification of surviving axons. The detailed procedure has been published before [14,15,44]. Briefly, the ON was exposed by removing the brain and post-fixed in situ using 2% glutaraldehyde/2% PFA in 0.1 M PB for 4 h on ice. Samples were then washed with 0.1 M PB 3 times, 10 min each wash. The ONs were then carefully dissected out and rinsed with 0.1 M PB 3 times, 10 min each wash. They were then incubated in 1% osmium tetroxide in 0.1 M PB for 1 h at room temperature followed by washing with 0.1 M PB for 10 min and water for 5 min. ONs were next dehydrated through graded ethanol, infiltrated in propylene oxide and epoxy, and embedded in epoxy at 60 °C for 24 h. Semi-thin sections (1 µm) were cut on an ultramicrotome (EM UC7, Leica) and collected 2 mm distal to the eye. The semi-thin sections were attached to glass slides and stained with 1% para-phenylenediamine (PPD) in methanol: isopropanol (1:1) for 35 min. After rinsing 3 times with methanol: isopropanol (1:1), coverslips were applied with PermOUNT Mounting Medium (Electron Microscopy Sciences, Hatfield, Pennsylvania). PPD stains all myelin sheaths, but darkly stains the axoplasm only of degenerating axons, which allows us to differentiate surviving axons from degenerating axons [47]. The whole ON were imaged with a 100× lens of a Keyence fluorescence microscopy to cover the entire area of the ON without overlap. Four areas of 108 µm × 144 µm were cropped, and the surviving axons within the designated areas counted manually with Fiji/ImageJ. After counting all the images taken from a single nerve, the mean of the surviving axon number was calculated for each ON. The investigators who counted the axons were masked to the treatment of the samples.

Anterior segments and retina cross sections and H & E and Trichrome Staining. Monkey eyes were enucleated and immediately fixed in 10% formalin for 36 h at room temperature. They were processed through graded alcohol and xylene, then infiltrated and embedded in paraffin. Six-micron sections were taken and stained with Hematoxylin & Eosin (H & E) to look at the cell nuclei, extracellular matrix, and cytoplasm using Nikon Eclipse (E800) microscope. Standard protocol was followed to stain these slides. The Trichrome kit was purchased from Abcam (ab 150686) to study collagenous connective tissue in sections. Slides were deparaffinized and incubated in preheated Bouin's fluid for an hour and rinsed in water. They were then incubated in Weigert's Iron Hematoxylin for 5 min, rinsed in water again and then incubated in Biebrich Scarlet/Acid Fuchsin solution for 15 min. They were rinsed in water again. Sections were then differentiated in phosphotungstic acid solution for 10–15 min (or until collagen is not red), incubated in Aniline Blue solution for 5–10 min and rinsed in water. Acetic acid solution was applied to these sections for 3–5 min, and slides were then dehydrated in alcohol, cleared in xylene, and mounted with CytoSeal 60 (from Electron Microscopy Sciences, 18006). This stain shows a stronger collagen stain (blue green stain) in glaucomatous eye than the control eye.

Statistical analyses. GraphPad Prism 7 was used to generate graphs and for statistical analyses. Data are presented as means ± s.e.m. Student's t-test was used for two groups comparison and One-way ANOVA with post hoc test was used for multiple comparisons.

5. Patents

A provisional patent application has been submitted by Stanford Office of Technology Licensing for SOHU animal glaucoma model in NHP.

Supplementary Materials: The supporting information can be downloaded at: <https://www.mdpi.com/article/10.3390/ijms232415896/s1>.

Author Contributions: Designed the experiments, Y.H., A.M. and F.F.; performed surgeries and eye exams, A.M.; processed the samples, F.F., P.Z., H.H., X.F., L.L. and R.D.; analyzed the data and prepared the manuscript, Y.H., F.F. and A.M. All authors have read and agreed to the published version of the manuscript.

Funding: Y.H. is supported by [CNPRC Pilot Grant, NIH grants], grant number [EY031063, EY024932, EY023295, EY028106, and EY032518], and grants from [Glaucoma Research Foundation (CFC3), BrightFocus Foundation, Chan Zuckerberg Initiative Neurodegeneration Collaborative Pairs Pilot Projects, Stanford SPARK program, and Stanford Center for Optic Disc Drusen]. We are grateful for an unrestricted grant from [Research to Prevent Blindness and NEI P30 EY026877 to the Department of Ophthalmology, Stanford University].

Institutional Review Board Statement: The study was conducted in accordance with the Guidelines of the Association for Research in Vision and Ophthalmology Statement for the Use of Animals in Ophthalmic and Vision Research, and approved by Institutional Animal Care and Use Committee of University of California Davis (protocol number 21417) and Stanford University (protocol number 33697).

Data Availability Statement: All data generated or analyzed during this study are included in this published article (and its Supplementary Information files).

Acknowledgments: We thank Jeffrey Goldberg, Jie Zhang, Xin Duan, Derek Welsbie, Anna La Torre Vila, and Alan Tessler for critical discussion.

Conflicts of Interest: The authors declare no conflict of interest.

References

1. Howell, G.R.; Libby, R.; Jakobs, T.; Smith, R.S.; Phalan, F.C.; Barter, J.W.; Barbay, J.M.; Marchant, J.K.; Mahesh, N.; Porciatti, V.; et al. Axons of retinal ganglion cells are insulted in the optic nerve early in DBA/2J glaucoma. *J. Cell Biol.* **2007**, *179*, 1523–1537. [[CrossRef](#)]
2. Tham, Y.C.; Li, X.; Wong, T.Y.; Quigley, H.A.; Aung, T.; Cheng, C.Y. Global prevalence of glaucoma and projections of glaucoma burden through 2040: A systematic review and meta-analysis. *Ophthalmology* **2014**, *121*, 2081–2090. [[CrossRef](#)] [[PubMed](#)]
3. Weinreb, R.N.; Leung, C.K.; Crowston, J.G.; Medeiros, F.A.; Friedman, D.S.; Wiggs, J.L.; Martin, K.R. Primary open-angle glaucoma. *Nat. Rev. Dis. Prim.* **2016**, *2*, 16067. [[CrossRef](#)] [[PubMed](#)]
4. Calkins, D.J. Adaptive responses to neurodegenerative stress in glaucoma. *Prog. Retin. Eye Res.* **2021**, *84*, 100953. [[CrossRef](#)] [[PubMed](#)]
5. Iyer, J.; Vianna, J.R.; Chauhan, B.C.; Quigley, H.A. Toward a new definition of glaucomatous optic neuropathy for clinical research. *Curr. Opin. Ophthalmol.* **2020**, *31*, 85–90. [[CrossRef](#)] [[PubMed](#)]
6. Burgoyne, C.F. A biomechanical paradigm for axonal insult within the optic nerve head in aging and glaucoma. *Exp. Eye Res.* **2011**, *93*, 120–132. [[CrossRef](#)]
7. Calkins, D.J. Critical pathogenic events underlying progression of neurodegeneration in glaucoma. *Prog. Retin. Eye Res.* **2012**, *31*, 702–719. [[CrossRef](#)]
8. Heijl, A.; Leske, M.C.; Bengtsson, B.; Hyman, L.; Bengtsson, B.; Hussein, M.; Early Manifest Glaucoma Trial Group. Reduction of intraocular pressure and glaucoma progression: Results from the Early Manifest Glaucoma Trial. *Arch. Ophthalmol.* **2002**, *120*, 1268–1279. [[CrossRef](#)]
9. Garway-Heath, D.F.; Crabb, D.P.; Bunce, C.; Lascaratos, G.; Amalfitano, F.; Anand, N.; Azuara-Blanco, A.; Bourne, R.R.; Broadway, D.C.; Cunliffe, I.A.; et al. Latanoprost for open-angle glaucoma (UKGTS): A randomised, multicentre, placebo-controlled trial. *Lancet* **2015**, *385*, 1295–1304. [[CrossRef](#)]
10. Anderson, D.R. Collaborative normal tension glaucoma study. *Curr. Opin. Ophthalmol.* **2003**, *14*, 86–90. [[CrossRef](#)]
11. Wormald, R.; Virgili, G.; Azuara-Blanco, A. Systematic reviews and randomised controlled trials on open angle glaucoma. *Eye* **2019**, *34*, 161–167. [[CrossRef](#)] [[PubMed](#)]
12. Wareham, L.K.; Risner, M.L.; Calkins, D.J. Protect, Repair, and Regenerate: Towards Restoring Vision in Glaucoma. *Curr. Ophthalmol. Rep.* **2020**, *8*, 301–310. [[CrossRef](#)] [[PubMed](#)]
13. Beykin, G.; Norcia, A.M.; Srinivasan, V.J.; Dubra, A.; Goldberg, J.L. Discovery and clinical translation of novel glaucoma biomarkers. *Prog. Retin. Eye Res.* **2020**, *80*, 100875. [[CrossRef](#)] [[PubMed](#)]
14. Zhang, J.; Liu, L.; Huang, H.; Fang, F.; Webber, H.C.; Zhuang, P.; Dalal, R.; Tang, P.H.; Mahajan, V.; Sun, Y.; et al. Silicone oil-induced ocular hypertension and glaucomatous neurodegeneration in mouse. *eLife* **2019**, *8*, e45881. [[CrossRef](#)] [[PubMed](#)]
15. Zhang, J.; Fang, F.; Li, L.; Huang, H.; Webber, H.C.; Sun, Y.; Mahajan, V.; Hu, Y. A Reversible Silicon Oil-Induced Ocular Hypertension Model in Mice. *J. Vis. Exp.* **2019**, *153*, e60409. [[CrossRef](#)]
16. Fang, F.; Zhang, J.; Zhuang, P.; Liu, P.; Li, L.; Huang, H.; Webber, H.C.; Xu, Y.; Dalal, R.; Sun, Y.; et al. Chronic mild and acute severe glaucomatous neurodegeneration derived from silicone oil-induced ocular hypertension. *Sci. Rep.* **2021**, *11*, 9052. [[CrossRef](#)]
17. Ichhpujani, P.; Jindal, A.; Jay Katz, L. Silicone oil induced glaucoma: A review. *Graefe's Arch. Clin. Exp. Ophthalmol.* **2009**, *247*, 1585–1593. [[CrossRef](#)]
18. Kornmann, H.L.; Gedde, S.J. Glaucoma management after vitreoretinal surgeries. *Curr. Opin. Ophthalmol.* **2016**, *27*, 125–131. [[CrossRef](#)]

19. Harwerth, R.S.; Smith, E.L., 3rd. Rhesus monkey as a model for normal vision of humans. *Am. J. Optom. Vis. Sci.* **1985**, *62*, 633–641. [[CrossRef](#)]
20. Chen, L.; Zhao, Y.; Zhang, H. Comparative Anatomy of the Trabecular Meshwork, the Optic Nerve Head and the Inner Retina in Rodent and Primate Models Used for Glaucoma Research. *Vision* **2016**, *1*, 4. [[CrossRef](#)]
21. Burgoyne, C. The morphological difference between glaucoma and other optic neuropathies. *J. Neuro-Ophthalmol. Off. J. North Am. Neuro-Ophthalmol. Soc.* **2015**, *35* (Suppl S1), S8–S21. [[CrossRef](#)] [[PubMed](#)]
22. Burgoyne, C.F. The non-human primate experimental glaucoma model. *Exp. Eye Res.* **2015**, *141*, 57–73. [[CrossRef](#)] [[PubMed](#)]
23. Balcer, L.J.; Miller, D.H.; Reingold, S.C.; Cohen, J.A. Vision and vision-related outcome measures in multiple sclerosis. *Brain* **2014**, *138*, 11–27. [[CrossRef](#)] [[PubMed](#)]
24. Aktas, O.; Albrecht, P.; Hartung, H.P. Optic neuritis as a phase 2 paradigm for neuroprotection therapies of multiple sclerosis: Update on current trials and perspectives. *Curr. Opin. Neurol.* **2016**, *29*, 199–204. [[CrossRef](#)] [[PubMed](#)]
25. Costello, F.; Coupland, S.; Hodge, W.; Lorello, G.; Koroluk, J.; Pan, Y.I.; Freedman, M.S.; Zackon, D.H.; Kardon, R.H. Quantifying axonal loss after optic neuritis with optical coherence tomography. *Ann. Neurol.* **2006**, *59*, 963–969. [[CrossRef](#)]
26. Viswanathan, S.; Frishman, L.J.; Robson, J.G.; Harwerth, R.S.; Smith, E.L. The photopic negative response of the macaque electroretinogram: Reduction by experimental glaucoma. *Investig. Ophthalmol. Vis. Sci.* **1999**, *40*, 1124–1136.
27. Wilsey, L.; Gowrisankaran, S.; Cull, G.; Hardin, C.; Burgoyne, C.F.; Fortune, B. Comparing three different modes of electroretinography in experimental glaucoma: Diagnostic performance and correlation to structure. *Doc. Ophthalmol.* **2017**, *134*, 111–128. [[CrossRef](#)]
28. Coleman, D.J. Evaluation of ciliary body detachment in hypotony. *Retina* **1995**, *15*, 312–318. [[CrossRef](#)]
29. Flores-Sanchez, B.C.; Tatham, A.J. Acute angle closure glaucoma. *Br. J. Hosp. Med. (Lond)* **2019**, *80*, C174–C179. [[CrossRef](#)]
30. Lockwood, H.; Reynaud, J.; Gardiner, S.; Grimm, J.; Libertaux, V.; Downs, J.C.; Yang, H.; Burgoyne, C.F. Lamina Cribrosa Microarchitecture in Normal Monkey Eyes Part 1: Methods and Initial Results. *Investig. Ophthalmology Vis. Sci.* **2015**, *56*, 1618–1637. [[CrossRef](#)]
31. Yang, H.; Reynaud, J.; Lockwood, H.; Williams, G.; Hardin, C.; Reyes, L.; Stowell, C.; Gardiner, S.K.; Burgoyne, C.F. The connective tissue phenotype of glaucomatous cupping in the monkey eye—Clinical and research implications. *Prog. Retin. Eye Res.* **2017**, *59*, 1–52. [[CrossRef](#)] [[PubMed](#)]
32. He, L.; Yang, H.; Gardiner, S.K.; Williams, G.; Hardin, C.; Strouthidis, N.G.; Fortune, B.; Burgoyne, C.F. Longitudinal Detection of Optic Nerve Head Changes by Spectral Domain Optical Coherence Tomography in Early Experimental Glaucoma. *Investig. Ophthalmology Vis. Sci.* **2014**, *55*, 574–586. [[CrossRef](#)] [[PubMed](#)]
33. Downs, J.C.; Girkin, C.A. Lamina cribrosa in glaucoma. *Curr. Opin. Ophthalmol.* **2017**, *28*, 113–119. [[CrossRef](#)] [[PubMed](#)]
34. Hopkins, A.; Murphy, R.; Irnaten, M.; Wallace, D.M.; Quill, B.; O'Brien, C. The role of lamina cribrosa tissue stiffness and fibrosis as fundamental biomechanical drivers of pathological glaucoma cupping. *Am. J. Physiol. Physiol.* **2020**, *319*, C611–C623. [[CrossRef](#)]
35. Kim, J.-A.; Kim, T.-W.; Weinreb, R.N.; Lee, E.J.; Girard, M.J.A.; Mari, J.M. Lamina Cribrosa Morphology Predicts Progressive Retinal Nerve Fiber Layer Loss In Eyes with Suspected Glaucoma. *Sci. Rep.* **2018**, *8*, 738. [[CrossRef](#)]
36. Carelli, V.; La Morgia, C.; Ross-Cisneros, F.N.; Sadun, A.A. Optic neuropathies: The tip of the neurodegeneration iceberg. *Hum. Mol. Genet.* **2017**, *26*, R139–R150. [[CrossRef](#)]
37. Toosy, A.T.; Mason, D.F.; Miller, D.H. Optic neuritis. *Lancet Neurol.* **2014**, *13*, 83–99. [[CrossRef](#)]
38. Talman, L.S.; Bisker, E.R.; Sackel, D.J.; Long, D.A., Jr.; Galetta, K.M.; Ratchford, J.N.; Lile, D.J.; Farrell, S.K.; Loguidice, M.J.; Remington, G.; et al. Longitudinal study of vision and retinal nerve fiber layer thickness in multiple sclerosis. *Ann. Neurol.* **2010**, *67*, 749–760.
39. McKinnon, S.J. Glaucoma: Ocular Alzheimer's disease? *Front. Biosci.* **2003**, *8*, s1140–s1156. [[CrossRef](#)]
40. Chiasseu, M.; Vargas, J.L.C.; Destroismaisons, L.; Velde, C.V.; Leclerc, N.; Di Polo, A. Tau Accumulation, Altered Phosphorylation, and Missorting Promote Neurodegeneration in Glaucoma. *J. Neurosci.* **2016**, *36*, 5785–5798. [[CrossRef](#)]
41. Minegishi, Y.; Nakayama, M.; Iejima, D.; Kawase, K.; Iwata, T. Significance of optineurin mutations in glaucoma and other diseases. *Prog. Retin. Eye Res.* **2016**, *55*, 149–181. [[CrossRef](#)] [[PubMed](#)]
42. Wiggs, J.L.; Pasquale, L.R. Genetics of glaucoma. *Hum. Mol. Genet.* **2017**, *26*, R21–R27. [[CrossRef](#)] [[PubMed](#)]
43. Lin, K.H.; Tran, T.; Kim, S.; Park, S.; Stout, J.T.; Chen, R.; Rogers, J.; Yiu, G.; Thomasy, S.; Moshiri, A. Advanced Retinal Imaging and Ocular Parameters of the Rhesus Macaque Eye. *Transl. Vis. Sci. Technol.* **2021**, *10*, 7. [[CrossRef](#)] [[PubMed](#)]
44. Li, L.; Huang, H.; Fang, F.; Sun, Y.; Hu, Y.; Liu, L. Longitudinal Morphological and Functional Assessment of RGC Neurodegeneration After Optic Nerve Crush in Mouse. *Front. Cell. Neurosci.* **2020**, *14*, 109. [[CrossRef](#)]
45. Kwong, J.M.K.; Caprioli, J.; Piri, N. RNA Binding Protein with Multiple Splicing: A New Marker for Retinal Ganglion Cells. *Investig. Ophthalmology Vis. Sci.* **2010**, *51*, 1052–1058. [[CrossRef](#)]
46. Rodriguez, A.R.; Müller, L.P.D.S.; Brecha, N.C. The RNA binding protein RBPMS is a selective marker of ganglion cells in the mammalian retina. *J. Comp. Neurol.* **2013**, *522*, 1411–1443. [[CrossRef](#)]
47. Smith, R.S. *Systematic Evaluation of the Mouse Eye: Anatomy, Pathology, and Biomethods*; CRC Press: Boca Raton, FL, USA, 2002; p. 366.